# On the Turbulent Mixing Length in the Oceanic Boundary Layer

MILES G. MCPHEE

*McPhee Research Company, Naches, Washington*

(Manuscript received 23 November 1993, in final form 25 January 1994)

ABSTRACT

Turbulence measurements from under drifting pack ice illustrate the distribution of turbulent mixing length in the well-mixed layer of the upper ocean. Mixing length ($\lambda \equiv K/u_*$, where $K$ and $u_*$ are the *local* eddy viscosity and square root of Reynolds stress, respectively) is found to vary inversely with wavenumber at the peak in the weighted vertical velocity variance spectrum: $\lambda = c_s/k_{max}$. This relation provides an empirical tool for making local estimates of eddy viscosity if the Reynolds stress is known, or alternatively, deriving fluxes via the *inertial–dissipation* method in the outer part of the rotational boundary layer. The vertical structure of $\lambda$ is described for conditions of (i) neutral stratification (negligible surface buoyancy flux) under thick ice, (ii) stable stratification under rapidly melting ice, and (iii) statically unstable conditions from intense freezing. The last example, obtained during the 1992 Lead Experiment, included direct measurements of turbulent salinity flux, $\langle w'S' \rangle$. As an analog to Monin–Obukhov similarity for the atmospheric surface layer, a simple algorithm is developed for calculating $\lambda$ in the mixed layer in terms of displacement from the interface, $z$; boundary values of friction velocity, $u_{*0}$, and buoyancy flux, $\langle w'b' \rangle_0$; the planetary length scale, $u_{*0}/|f_{cor}|$ (for neutral and stable conditions); and mixed layer depth, $|z_{ml}|$ (unstable conditions). A simple numerical model demonstrates the algorithm by simulating a hypothetical example of intense wind stirring in the wintertime Weddell Sea.

## 1. Introduction

The purpose of this paper is to formulate a relatively simple framework for describing the mixing length distribution in the oceanic mixed layer. Mixing length, $\lambda$, is defined by relating the vertical flux of momentum (turbulent Reynolds stress, $\langle w'\mathbf{u}' \rangle$) to the gradient of mean velocity, $\mathbf{U}$:

$$\langle w'\mathbf{u}' \rangle = -K\frac{\partial \mathbf{U}}{\partial z} \equiv -u_*\lambda\frac{\partial \mathbf{U}}{\partial z}, \qquad (1)$$

where primes denote deviatory quantities in the usual Reynolds ensemble averaging sense, $K$ is the *eddy viscosity,* and $u_*$ and $\lambda$ describe, respectively, the overturning speed of the *energy-containing* turbulent eddies and the vertical distance over which they are effective at diffusing momentum. While the vector relationship (1) is an approximation to a fourth-order tensor equation, valid only under fairly restrictive assumptions (Hinze 1975, chapter 1), first-order closure via scalar eddy viscosity often provides a useful and fairly accurate description in shear flows where the gradient is mainly vertical (e.g., Tennekes and Lumley 1972).

Eddy viscosity and diffusivity of heat and water vapor are reasonably well understood in the atmospheric *surface layer,* which is generally taken to mean that part of the planetary boundary layer (PBL) where turbulent fluxes vary little from their surface values, and where rotation terms involving the Coriolis parameter, $f_{cor}$, are relatively unimportant. An obvious scale velocity in the surface layer is $u_{*0} = \sqrt{\tau_0}$, the square root of kinematic stress at the interface. For the atmospheric surface layer, mixing length $\lambda$ follows directly from Monin–Obukhov similarity theory for the nondimensional wind profile:

$$\phi_m = \frac{\kappa z}{u_{*0}}\frac{\partial U}{\partial z} = \phi_m(\zeta),$$

where $\zeta = z/L_0$, $\kappa$ is von Kármán's constant,

$$L_0 = \frac{u_{*0}^3}{\kappa\langle w'b' \rangle_0}$$

is the Obukhov length, and $\langle w'b' \rangle_0$ is the buoyancy flux at the boundary. Since the momentum flux is $u_{*0}^2$,

$$\lambda = \kappa z/\phi_m.$$

Using, for example, the empirical results of Businger et al. (1971), a fairly comprehensive expression for the mixing length in the surface layer is given by

$$\lambda = \begin{cases} \dfrac{\kappa z}{1 + 4.7\zeta}, & \zeta \geq 0 \\ \kappa z(1 - 15\zeta)^{1/4}, & \zeta < 0. \end{cases} \qquad (2)$$

In the neutral limit ($L_0 \to \pm\infty$) mixing length is proportional to $z$.

*Corresponding author address:* Dr. Miles G. McPhee, McPhee Research Company, 450 Clover Springs Road, Naches, WA 98937.

Tennekes (1973) suggested a somewhat arbitrary outer limit of $0.03u_{*0}/f_{cor}$ for the surface layer. By this reckoning, typical surface-layer extents in the atmosphere and ocean are 60 m and 2 m, respectively, and most of the ocean mixed layer lies beyond the surface layer in the region called the *outer* or Ekman layer.[1] In the outer part of the PBL rotation is important, and the well-mixed layer is usually bounded by a steep density gradient. Thus, in addition to distance from the boundary and the Obukhov length, at least two new length scales should be considered: the *planetary scale*, $u_{*0}/|f_{cor}|$, and the depth of the mixed layer (or inversion height), $-z_{ml}$. The problem of turbulence scales is more complex in the outer layer, and the usual approaches have been either to parameterize the mixing process in terms of bulk energetics of the flow (e.g., Kraus and Turner 1967) or to numerically solve the time-dependent boundary-layer equations over a finely spaced grid with some closure assumption for the covariance terms (e.g., Mellor and Yamada 1982) or turbulent kinetic energy (TKE) balance (e.g., Omstedt and Svensson 1984). Here we consider a middle ground by seeking a set of expressions analogous to (2) for mixing length in the oceanic PBL in terms of $u_{*0}$, $\langle w'b'\rangle_0$, $f_{cor}$, and $z_{ml}$.

The problem is that in the well-mixed layer of the ocean there are few data for relating the fluxes and mean gradients. Near the surface of the open ocean, waves make it technically very difficult to measure three-dimensional velocity fields required for direct flux measurements. It is also hard to detect small gradients in velocity and scalar fields characteristic of the mixed layer. Turbulence in the open ocean is usually measured at small scales, using high-frequency response microstructure probes (e.g., Gregg 1987; Hopfinger 1987). Dissipation of turbulent kinetic energy (or temperature variance) is estimated from the microstructure measurements, then used in a simplified form of the TKE equation to estimate heat or momentum flux (e.g., Moum 1990). Most of the reported microstructure measurements are from the stratified thermocline below the mixed layer where buoyancy and internal waves are important [but see, e.g., Shay and Gregg (1986) for microstructure measurements in a convecting mixed layer]. Although there appears to be no clear consensus on the proper scaling for turbulence in the pycnocline (Gargett 1990), two length scales often associated with fluxes (or, equivalently eddy viscosity or diffusivity) in stratified flow are the Osmidov scale, $L_{OS} = \epsilon^{1/2}/N^{3/2}$, where $\epsilon$ is TKE dissipation rate and $N$ is the local buoyancy frequency; and the Thorpe scale, which is a measure of the vertical displacements required to bring parcels of fluid in a density profile with inversions back to a statically stable state (Dillon 1982). Both scales depend on an underlying density gradient and are thus meaningless in a neutrally stratified mixed layer.

By comparison with the open ocean, it is relatively easy to deploy sensitive instruments in the upper ocean under pack ice (once the logistic hurdle of operating in polar regions is crossed). In the past several years we have measured turbulent fluxes directly using eddy correlation techniques in the oceanic PBL that forms in response to wind-driven drift at a number of manned ice stations in the Arctic and Antarctic (e.g., McPhee et al. 1987; McPhee and Kantha 1989; McPhee 1992; McPhee and Martinson 1994). Turbulence measurements in or near the surface layer under sea ice have also been reported by Langleben (1982) and Shirasawa (1986). Although point measurements of flux at a few levels in the boundary layer are not enough in general to define the distribution of mixing length, recent work has suggested a promising method for extracting the dominant length scale directly from the peak in the weighted spectrum of vertical velocity (McPhee and Martinson 1994). This technique makes it possible to investigate the vertical structure of mixing length without having to measure the mean velocity shear at particular levels.

The paper is organized as follows. Section 2 presents data from three different times and projects, when the PBL was (i) neutrally stable under thick pack ice, (ii) stabilized by rapid melting in the marginal ice zone, and (iii) statically destabilized by freezing in an open lead. A brief digression describes how to use the measured length scale to estimate fluxes via the *inertial–dissipation* method adapted to the outer boundary layer. In section 3, the measurements are interpreted in terms of extension to a similarity theory (McPhee 1981). As an outer-layer analog to the surface-layer equations (2), an algorithm (essentially a flow chart) is presented for computing $\lambda$ in the mixed layer, based on the new results for the unstable boundary layer and on previous similarity scaling (McPhee 1981) for stable and neutral boundary layers. The approach is demonstrated heuristically with a numerical model meant to mimic some aspects of intense storm stirring in the winter Weddell Sea. Results are summarized in section 4.

The spirit here is exploratory. Compared with the database available for the atmospheric surface layer, our sample is minuscule: the unstable parameterization, for example, is based entirely on a few hours of data at the edge of an Arctic lead, when it was possible for the first time to directly measure salinity flux as well as Reynolds stress. Nonetheless, these measurements provide a starting point not previously available for the ocean.

[1] The *surface* layer usage here, which conforms with atmospheric convention, should not be confused with oceanographic usage that refers to both regions as the *surface mixing* layer.

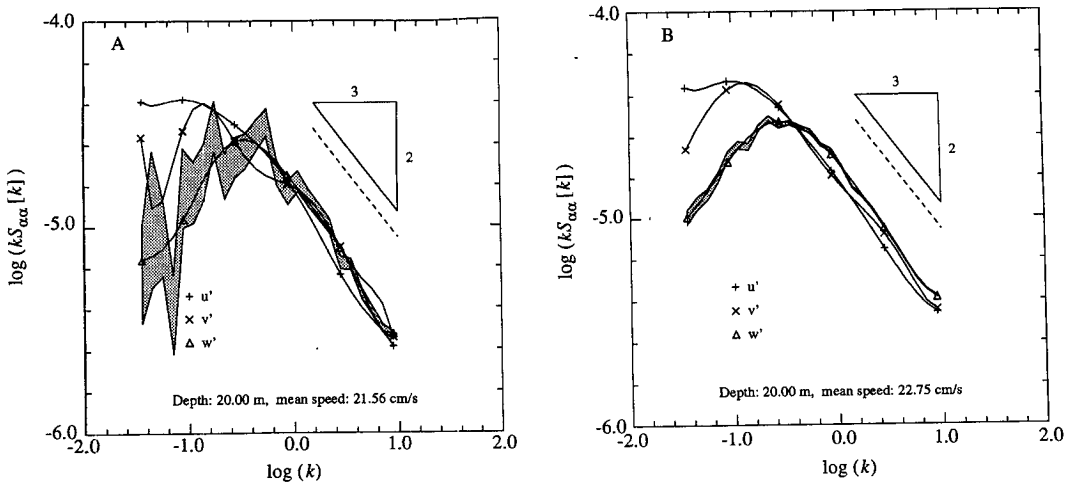


FIG. 1. (a) Weighted spectra (i.e., power spectral density multiplied by wavenumber) for downstream ($u'$), cross-stream ($v'$), and vertical ($w'$) deviatory velocities for a 1-h time series during a storm at ISW-1. The spectra have been fitted with a seventh-order polynomial. The shaded area represents the 95% confidence limit for the $w$ spectrum, as described in the text, and the dashed line indicates 4/3 spectral separation. (b) As in (a) except averaged in wavenumber bins over 12 h.

## 2. Measurements of mixing length

### a. *Neutrally stable flow: Ice Station Weddell*

During the joint U.S./Russian Ice Station Weddell-1 (ISW Group 1993), we suspended a mast beneath multiyear pack ice in the western Weddell Sea on which were mounted six turbulence instrument clusters (TICs), each sampling three components of velocity plus temperature and salinity at levels ranging from 4 to 24 m beneath the ice–ocean interface. Besides providing mean values at several levels simultaneously, the system samples at high enough frequencies to be well within the inertial subrange for turbulent velocity and temperature fluctuations, and thus measures momentum flux (the Reynolds stress tensor) and heat flux directly (e.g., McPhee 1992).

In late March 1992, a storm blew the ice pack surrounding ISW-1 rapidly northward, setting up a boundary layer within the mixed layer that was "well behaved" in the sense that Ekman spirals in both mean velocity and Reynolds stress were observed throughout. Mean turbulent structure during the storm, as described by McPhee and Martinson (1994), suggested a length scale associated with the wavenumber at the peak in the weighted vertical velocity spectrum as an estimate of mixing length. Here we review the spectra calculations and elaborate on the spectral peak method of estimating $\lambda$.

Velocity and temperature spectra were calculated from the storm data by forming 1-h time series, performing quality checks to ensure that all current meter components were turning, then rotating the velocity vectors into a "streamline" coordinate system aligned with the mean velocity vector, so that the cross-stream ($v$) and vertical ($w$) components have zero mean, and the average downstream ($u$) component is $U$. The time series were Fourier transformed, and spectral components calculated by smoothing the periodogram with one pass of a modified Daniell smoother of halfwidth 2 (Bloomfield 1976). The spectral components were then averaged in evenly spaced bins of $\log k$, where $k$ is the angular wavenumber: $k = 2\pi f/U$ obtained from the frequency, $f$, and the mean flow speed. These spectra may then be averaged for longer time periods, using the common wavenumber base. The 1-h time series were overlapped by half to provide better statistics for the high wavenumber (inertial subrange) end of the spectrum. To identify spectral peaks and inertial subrange levels objectively, the averaged spectra were fitted with seventh-order polynomials in the range $-1.5 < \log(k) < 1$. Similar techniques were used for all the spectra calculations discussed below. Examples are demonstrated by spectra from an individual 1-h time series (Fig. 1a) and from spectra averaged for 12 h (Fig. 1b), 20 m below the ice at ISW-1. The shaded confidence interval around the vertical spectrum gives some indication of how well the polynomial fit describes the actual spectral estimates. Note that in the longer average, the polynomial fits follow the average spectra closely. There is also a relatively well-defined region in which all three spectra fall off with the $-5/3$ slope ($-2/3$ in the weighted representation) and the ratios of both vertical and cross-stream spectra to the downstream spectrum are approximately 4/3. These characteristics are generally associated with isotropic turbulence in the inertial subrange.

Busch and Panofsky (1968) analyzed a number of wind spectra from the atmospheric surface layer under

varying conditions of surface buoyancy flux. Among other results, they found that weighted vertical wind velocity spectra (but not longitudinal or cross-stream spectra), normalized by kinematic surface stress, could be described fairly well by a simple function of nondimensional wavenumber, $\omega = k|z|$ (this definition differs from theirs by a factor of $2\pi$):

$$\frac{kS_{ww}(k)}{u_*^2} = \frac{A(\omega/\omega_m)}{1 + 1.5(\omega/\omega_m)^{5/3}}, \qquad (3)$$

where $S_{ww}(k)$ is the power spectral density of the vertical component. For neutrally stable and unstable surface layers, they estimated the constants $A$ and $\omega_m$ to be 1.075 and 2.0, respectively. Equation (3) implies that the wavenumber at the spectral peak varies inversely with $z$; thus in the neutral surface layer

$$\lambda = \kappa|z| = c_\lambda/k_{\max} = \frac{c_\lambda}{\omega_m}|z|, \qquad (4)$$

and from their results, $c_\lambda$ is approximately 0.8.

Since turbulence 4 m from the boundary should be governed approximately by surface-layer scaling, the mean $w$ spectrum from a 12-h period of relatively steady conditions is compared with the Busch–Panofsky formula (3) in Fig. 2. Dimensional spectral levels were calculated from the original nondimensional formula ($A = 1.075$, $\omega_m = 2.0$) by using surface stress derived from the observed Reynolds stress at 4 m, assuming an exponential falloff (McPhee and Martinson 1994). Although the original formula works well, closer correspondence to the measured spectrum in the vicinity of the spectral peak is obtained with minor changes to the coefficients: $A = 1.01$, $\omega_m = 2.14$. The larger nondimensional peak wavenumber implies a slightly larger value of 0.85 for $c_\lambda$.

McPhee and Martinson (1994) used bulk properties of the boundary layer (the Ekman stress spiral, and mean heat flux and temperature gradient) averaged over the storm to estimate eddy viscosity and scalar diffusivity. These results compared favorably with eddy viscosity $K = \lambda_{\text{peak}} u_*$ derived from the wavenumber at the peak in the $w$ spectrum, and from the TKE dissipation. The analysis is extended here by adding a *local* estimate of the mixing length associated with heat transport, obtained from the dissipation of temperature variance. If the limitations of the TKE and temperature variance assumptions are recognized, the general framework provides a method for estimating fluxes from the wavenumber spectra for vertical velocity and temperature fluctuations alone, as demonstrated below. It is closely related to the *inertial-dissipation* method used in atmospheric surface-layer studies (e.g., Edson et al. 1991) and near the seafloor in tidal flows (Gross and Nowell 1985) except for the way in which the length scale is determined. The basic idea is that the steady, horizontally homogeneous TKE equation expresses a balance among four terms: production of turbulent kinetic energy by mean shear ($P_S$) plus production (or consumption) by buoyancy ($P_b$) on one side, balanced by vertical divergence of TKE flux and pressure velocity covariance ($D$) plus molecular dissipation ($\epsilon$) on the other:

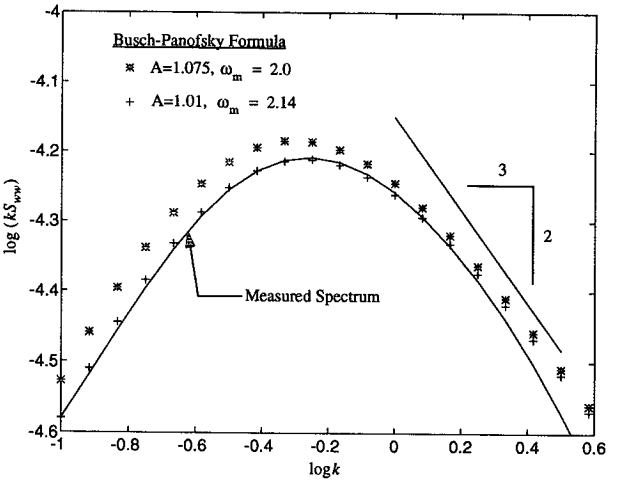


FIG. 2. Comparison of the measured $w$ spectrum at 4 m during the ISW-1 storm with the empirical "universal" surface-layer spectrum of Busch and Panofsky (1968), with two different sets of coefficients. Asterisks mark the original formula.

$$\underbrace{-\langle u'w'\rangle \frac{\partial U}{\partial z} - \langle v'w'\rangle \frac{\partial V}{\partial z}}_{P_S} \underbrace{- \frac{g}{\rho}\langle \rho' w'\rangle}_{P_b} = \underbrace{\frac{\partial}{\partial z}\left(\frac{1}{2}\langle u_i' u_i' w'\rangle + \frac{1}{\rho}\langle p' w'\rangle\right)}_{D} + \underbrace{\nu\left\langle \frac{\partial u_i'}{\partial x_i}\frac{\partial u_i'}{\partial x_i}\right\rangle}_{\epsilon}, \qquad (5)$$

where primes denote deviatory quantities and repeated indices imply summation [see, e.g., Tennekes and Lumley (1972) for discussion of the various terms in the TKE budget]. As defined here, buoyancy production is the negative of buoyancy flux. The equation is usually further simplified by assuming that divergence in vertical transport of TKE and divergence in the pressure velocity correlation either cancel or are both negligible. Near the under-ice boundary, the most questionable assumption in using the simplified equation, $P_S + P_b = \epsilon$, is probably horizontal homogeneity. Pack ice is usually hydraulically rough, with large effective roughness length comprising protrusions on the ice underside at numerous scales (except in heavily deformed ice, the most apt atmospheric analog is flow over small hills). It is not uncommon to find that

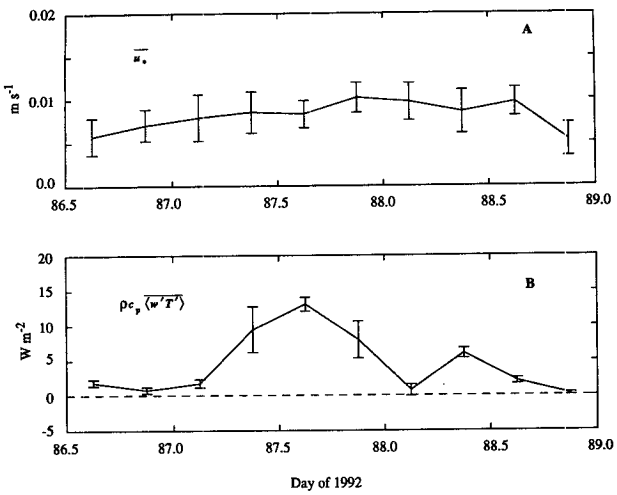


FIG. 3. (a) Average friction velocity [$u_* = (\langle u'w' \rangle^2 + \langle v'w' \rangle^2)^{1/4}$] from turbulence instrument clusters at 4, 8, 16, 20, and 24 m below the ice during a storm at ISW-1. Error bars are twice the sample standard deviation. Data were averaged in 6-h blocks. (b) Turbulent heat flux; otherwise as in (a).

Reynolds stress increases with distance from the interface (McPhee et al. 1987) as the flow adjusts to larger roughness elements over a longer averaging path. A consequence of this is that for shallow measurements, we often find that TKE production and dissipation are significantly different (e.g., McPhee and Smith 1976). As the measurement level moves away from the interface, the flow responds to the total roughness, more closely satisfying horizontal homogeneity.

The question of boundary-layer stability during the ISW-1 storm was considered by McPhee and Martinson (1994). Latent heat exchange at the interface, either freezing or melting, probably did not exceed 20 W m$^{-2}$ during the ISW-1 storm. With this setting upper and lower bounds on salinity flux at the interface, we found that the magnitude of the Obukhov length based on surface flux conditions was greater than 300 m, and that buoyancy production in the TKE equation ($|\langle w'b' \rangle_0| < 1.3 \times 10^{-8}$ m$^2$ s$^{-3}$) was negligible in the depth range of the instrument mast.

If it is further assumed that the local mean shear may be expressed as turbulent scale velocity divided by mixing length; then the TKE equation reduces to

$$\frac{u_*^3}{\lambda_\epsilon} = \epsilon. \tag{6}$$

An equation analogous to the TKE equation may be written for temperature variance, and under the same assumptions, it may be simplified to a balance between temperature variance production and temperature variance dissipation, $\epsilon_T$:

$$\left| \langle w'T' \rangle \frac{\partial T}{\partial z} \right| = \frac{\langle w'T' \rangle^2}{u_* \lambda_T} = \epsilon_T. \tag{7}$$

Dissipations are obtained from spectral levels ($S_{ww}$, $S_{TT}$) in the inertial subrange where the energy (or temperature variance) cascade is independent of both the large and small scales governing the flow (Hinze 1975):

$$\epsilon^{2/3} = \frac{3}{4\alpha_\epsilon} S_{ww}(k) k^{5/3} \tag{8}$$

and

$$\epsilon_T = \frac{\epsilon^{1/3}}{\alpha_T} S_{TT}(k) k^{5/3}, \tag{9}$$

where $\alpha_\epsilon = 0.51$ and $\alpha_T = 0.79$ are the Kolmogorov constants for TKE and temperature variance, respectively, using numerical values suggested by Edson et al. (1991) for flows in which production and dissipation balance. The inertial subrange was identified by finding the lowest wavenumber where the slope of the fitted, weighted $w$ spectrum first matched $-2/3$.

With measurements of $u_*$, $\langle w'T' \rangle$, $\epsilon$, and $\epsilon_T$, (6) and (7) provide a means of making a purely *local* estimate of mixing length independent of the peak in the $w$ spectrum. Of the 6-h averages, only those for which the vertical mean heat flux exceeded 5 W m$^{-2}$ (Fig. 3) were used, in order to include $\lambda_T$ in the comparison. Results are summarized in Table 1, which lists the length scales obtained from the $w$ and $T$ spectra, along with the length scale $\lambda_{peak} = 0.85/k_{max}$. Looking first at the length scale from TKE dissipation ($\lambda_\epsilon$), the

TABLE 1. Turbulence properties and derived mixing length estimates at five levels during a storm at ISW-1. Mixing lengths are $\lambda_\epsilon$, from measured friction velocity and inertial subrange dissipation (Eq. 6); $\lambda_T$, from inertial subrange TKE and temperature variance dissipation, and measured $u_*$ (Eq. 7); and $\lambda_{peak} = c_\lambda/k_{max}$.

| Depth (m) | $u_*$ (cm s$^{-1}$) | $\rho c_p \langle w'T' \rangle$ (W m$^{-2}$) | $\epsilon$ (m$^2$ s$^{-3}$($\times 10^7$)) | $\lambda_\epsilon$ (m) | $\epsilon_T$ (K$^2$ s$^{-1}$($\times 10^{10}$)) | $\lambda_T$ (m) | $\lambda_{peak}$ (m) |
|---|---|---|---|---|---|---|---|
| 4 | 1.14 | 8.2 | 7.8 | 1.9 | 2.4 | 1.8 | 1.5 |
| 8 | 1.05 | 9.0 | 4.4 | 2.7 | 2.0 | 2.6 | 2.3 |
| 16 | 0.83 | 9.4 | 2.3 | 2.8 | 2.9 | 2.7 | 3.5 |
| 20 | 0.76 | 9.9 | 1.8 | 3.5 | 3.3 | 2.8 | 3.4 |
| 24 | 0.66 | 9.1 | 1.4 | 2.2 | 5.6 | 2.5 | 3.0 |

agreement with $\lambda_{peak}$ is fairly good, especially considering the significant decrease in dissipation with depth. Since the 4-m level is still marginally within the logarithmic surface layer, an estimate of TKE production is $P = u_*^3/(\kappa|z|)$, which is $9.3 \times 10^{-7}$ W kg$^{-1}$ (m$^2$ s$^{-3}$), or about 20% larger than dissipation estimated from the inertial subrange, suggesting possible influence of the neglected transport terms. The length scale based on the spectral peak at 4 m is close to the surface-layer scale, $\kappa|z| = 1.6$ m. The thermal length scale, $\lambda_T$, is calculated from measured stress, heat flux, and temperature spectra; hence, it is essentially independent of the other two scales. Despite the small heat flux magnitudes, $\lambda_T$ is comparable to the others, and in fact seems to exhibit less vertical variability.

There is obvious practical utility for developing an inertial–dissipation method for estimating flux magnitude in the outer part of the oceanic boundary layer. In general, it is considerably more difficult to measure the three-dimensional velocity vector and $\langle w'T' \rangle$ than it is the $w$ and $T$ spectra. High-resolution acoustic Doppler current profilers, for example, may soon provide more-or-less continuous vertical velocity data through most of the mixed layer. It is relatively easy to measure temperature frequency spectra, which combined with $w$ frequency spectra and mean horizontal speed would provide the data necessary to calculate $\lambda_{peak}$, $\epsilon$, and $\epsilon_T$. Flux magnitudes may then be estimated directly from (6) and (7) if buoyancy production is negligible, or with iterative corrections if it is not. The technique is demonstrated for turbulent stress in Fig. 4a, which shows the average measured stress at each level during the ISW-1 storm with that estimated exclusively from the $w$ spectrum; that is, $\tau = (\epsilon\lambda_{peak})^{2/3}$. There is reasonable agreement through the outer layer. At 4 m, the spectral method departs somewhat further from observed, but this is not surprising in light of the difference between production and dissipation mentioned above. The square symbols show stress estimated from dissipation assuming that the length scale continues to increase with distance from the interface; that is, $\tau_{sl} = (\epsilon\kappa|z|)^{2/3}$. The discrepancy becomes obvious in the middle range of the mixed layer, where stress based on surface-layer scaling is overestimated by a factor of 2.

The spectral estimate for heat flux magnitude follows from the temperature variance equation: $|\langle w'T' \rangle|_\epsilon = (u_{*\epsilon}\lambda_{peak}\epsilon_T)^{1/2}$. The comparison with measured heat flux magnitude is reasonably good (Fig. 4b). The spectral heat flux estimates based on surface-layer scaling (square symbols) also depart rapidly from measured values with increasing depth. Note that the spectral estimates for stress and heat flux magnitude depend only on the frequency spectra and mean speed (for Taylor's hypothesis). The Kolmogorov constants are taken from the atmospheric literature, and the length scale constant, $c_\lambda = 0.85$, comes from a slight modification to earlier atmospheric measurements based on the 4-m spectrum of Fig. 2.

### b. *Neutral to stable flow: Marginal Ice Zone Experiment*

Data from the 1984 Marginal Ice Zone Experiment (MIZEX) illustrate the effect of stabilizing surface buoyancy flux on turbulent length scales in the outer boundary layer. The summer experiment, done from a drifting floe in the marginal ice zone of the Greenland Sea, included the first direct measurements of turbulent heat flux in the ocean mixed layer (McPhee et al. 1987; Morison et al. 1987; McPhee and Kantha 1989). During part of the drift, a storm blew our instrumented floe rapidly south across an abrupt front in mixed layer temperature, apparently the remnant of an ice-edge eddy that existed before the storm. Over a few hours, mixed layer temperature rose from near freezing to almost a degree above freezing. The combination of wind stress and warm mixed layer led to rapid ice melt associated with strong upward oceanic heat flux (McPhee et al. 1987). Time series of temperature, salinity, and friction velocity 7 m below the ice are shown in Fig. 5. For consistency with the ISW-1 analysis, turbulence quantities and spectra were again averaged in 6-h segments from 1-h time series overlapped by half. During the storm period, the mixed layer was much shallower than at ISW-1, ranging from a maximum thickness of about 22 m at time 189.5 to less than 10 m after 191.25 (see McPhee et al. 1987, Fig. 9).

Comparing a 6-h sample in Fig. 5 centered at 191.125 after crossing the front with an earlier sample at 189.875 shows that friction velocity at 7 m was almost identical (0.012 m s$^{-1}$), but water temperature had changed by about 1 K, accompanied by a large increase in upward turbulent heat flux and rapid melting at the ice–ocean interface. In polar mixed layers, freshwater influx (upward $\langle w'S' \rangle_0$) dominates the density structure, stabilizing the PBL. With rapid melting, gravity should thus reduce the vertical extent of the largest eddies. Spectra from 7 m below the ice (Fig. 6) suggest that spectral peaks did in fact shift toward higher wavenumber (smaller scales) after the rapid melting began. A comparison of the distribution of friction velocity and $\lambda_{peak}$ with depth is shown in Fig. 7. At 4 and 7 m there is a substantial reduction in mixing length after crossing the front, but only minor change at shallower depth.

Is the qualitative explanation for the reduction in $\lambda_{peak}$ consistent with the turbulence energetics? To address this question, buoyancy flux inferred from upward heat flux (Fig. 8a) was compared with TKE dissipation and shear production based on $\lambda_{peak}$ (Fig. 8b). Each plot includes horizontal lines representing the mean values before and after crossing the temperature front. Whereas the mean dissipation level remains relatively constant across the front, there is a significant

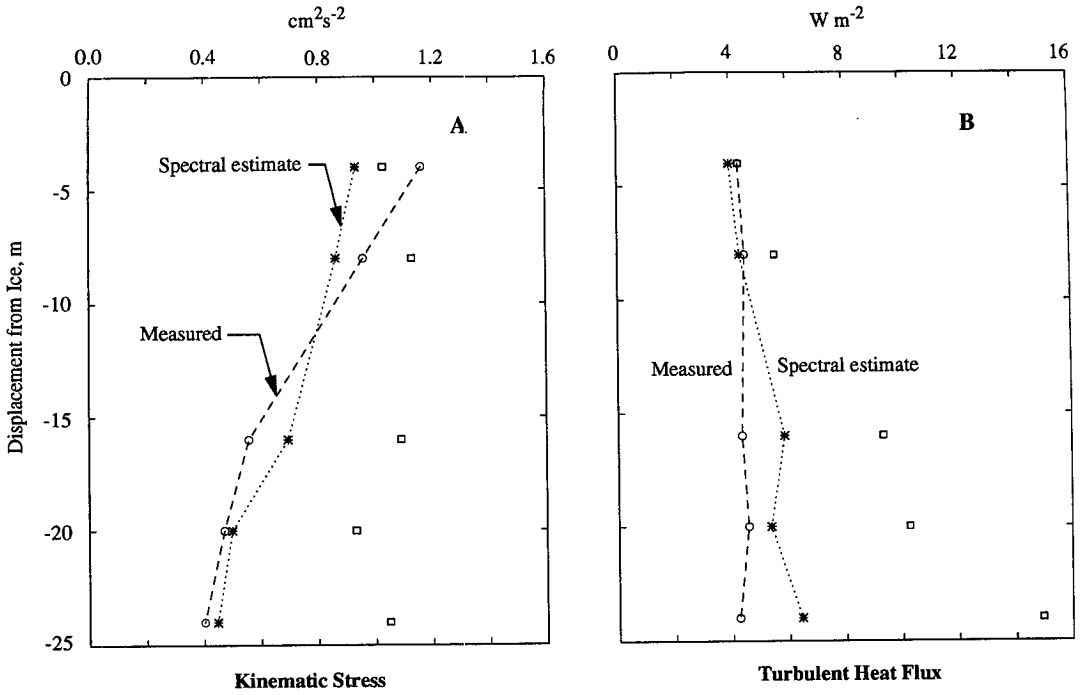


FIG. 4. (a) Average kinematic Reynolds stress during ISW-1 storm for all 6-h averages when the mean turbulent heat flux exceeded 5 W $m^{-2}$ (circles connected by dashed curve). Stress estimated from spectral levels in the inertial subrange using the turbulent length scale obtained from the peak in the weighted $w$ spectrum (asterisks connected by dotted curve), and using the turbulent length scale based on surface-layer scaling, $\kappa|z|$ (squares). (b) As in (a) except for turbulent heat flux. The spectral estimates are obtained from the $w$ and $T'$ variance spectra.

increase in shear production. Suppose that the TKE balance (5) is expressed as

$$\frac{u_*^3}{\lambda_{\text{peak}}} + P_{\text{other}} = \epsilon, \tag{10}$$

where $P_{\text{other}}$ represents another sink for TKE besides dissipation since in each case shear production is larger than dissipation; $P_{\text{other}}$ could involve a number of factors, but a likely source is stabilizing surface buoyancy flux. On the cold side of the front, water temperature was near freezing, so melting at the ice–ocean interface caused by upward oceanic heat flux was small. A steady decrease in salinity (Fig. 5b) suggests substantial input of freshwater to the top of the water column from melting at the upper surface of the ice and within the ice, but this might also have resulted from advection in an existing north–south salinity gradient. Before crossing the front, the mean value of $P_{\text{other}}$ was about $-0.12 \times 10^{-6}$ W $kg^{-1}$; after crossing its mean value was about $-0.38 \times 10^{-6}$ W $kg^{-1}$. It seems reasonable to ascribe the difference ($\Delta P = -0.26 \times 10^{-6}$ W $kg^{-1}$) to buoyancy flux from melting at the ice–ocean interface in response to increased oceanic heat flux:

$$\langle w'b' \rangle_0 = -\Delta P = \frac{g}{\rho}(\beta_S \langle w'S' \rangle_0 - \beta_T \langle w'T' \rangle_0), \tag{11}$$

where $\beta_S$ is the saline contraction coefficient and $\beta_T$ is the thermal expansion coefficient. The ducted conductivity meters used during MIZEX were not capable of resolving the salinity variance spectrum into the inertial subrange; hence direct measurements of $\langle w'S' \rangle$ were not made. However, if the upward heat flux is absorbed entirely by melting at the interface, then to a good approximation salinity flux is related to heat flux by (McPhee 1992)

$$\langle w'S' \rangle_0 = \frac{S_{\text{ml}} - S_{\text{ice}}}{Q_L} \langle w'T' \rangle_0, \tag{12}$$

where $S_{\text{ml}}$ and $S_{\text{ice}}$ are mixed layer and ice salinities, respectively, and $Q_L$ is the latent heat of fusion for saline ice divided by specific heat ($Q_L$ is equal to about 74 K for 4 psu ice). Substituting (12) into (11) with $\beta_T$ and $\beta_S$ evaluated at the mean temperature and salinity after crossing the front, the corresponding heat flux at the interface inferred from the TKE energy balance is $\rho c_p \langle w'T' \rangle_0 = 393$ W $m^{-2}$, which compares favorably with the difference in measured heat flux at 7 m: 372 W $m^{-2}$ (Fig. 8a). The close comparison may be partly fortuitous, given the chain of assumptions in this development; nevertheless, results of the energy analysis support the central premise that shear production can be estimated from the wavenumber at the peak in the vertical spectrum and the local Reynolds stress.

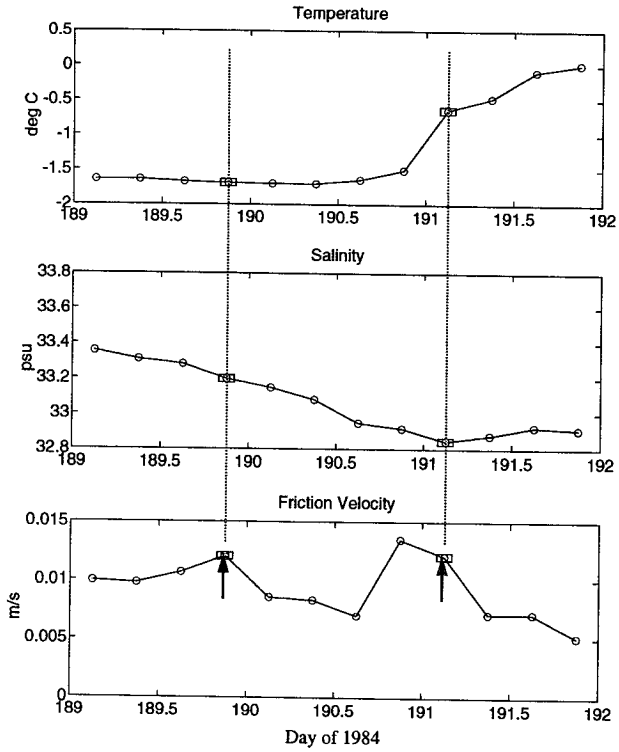


FIG. 5. Temperature, salinity, and friction velocity measured 7 m below the ice during the MIZEX 84 drift in Fram Strait. Data have been averaged in 6-h blocks. Arrows indicate samples on each side of an abrupt front in mixed layer temperature for which stress conditions are nearly identical.

An alternative hypothesis for the decrease in mixing length is that the existing mixed layer was shallower on the warm side of the front before the storm began, and that $\lambda$ was controlled more by $z_{ml}$ than by the interplay of $u_{*0}/|f_{cor}|$ and $L$. Although the example above and previous work (McPhee et al. 1987; McPhee 1990) have shown that the decrease was consistent with turbulence energetics, we do not know the characteristics of the mixed layer south of the front prior to our arrival there, and cannot discriminate between the two viewpoints with the MIZEX data alone. But by combining data from both MIZEX and ISW-1, we are able to examine response to a wide range of mixed layer depths. The record was searched for 6-h averages when upper ocean density was varied, but Reynolds stress was similar (Fig. 9). In each case, the surface melting or freezing was small (although perhaps not entirely negligible in the MIZEX case because of percolation through the ice as discussed above). The MIZEX example is from 7 m. Although the mixed layer at this time extended past a cluster mounted at 15 m, $\lambda_{peak}$ at 7 m was larger, thus probably more representative of the maximum value in the mixed layer. For comparison we used values from the ISW-1 mast at 16 m. This level instead of 8 m was chosen because $\kappa|z|$ scaling (about 3 m at 8-m displacement) might otherwise mask any dependence of the true maximum on $z_{ml}$. The peaks at 16 m represent the largest mixing lengths in the mixed layer. The two ISW-1 samples are almost identical, and the slightly smaller mixing length in the MIZEX sample likely results from weak surface buoyancy flux, as discussed above. If there is a dependence of $\lambda$ on mixed layer depth, it is weak.

### c. *Statically unstable flow: Lead Experiment*

During the 1992 Lead Experiment (LEADEX), a base camp was established on thick, multiyear ice over the Canadian Basin north of Alaska during late winter (16 March to 25 April). On several occasions, a number of instrumentation systems were airlifted by heli-

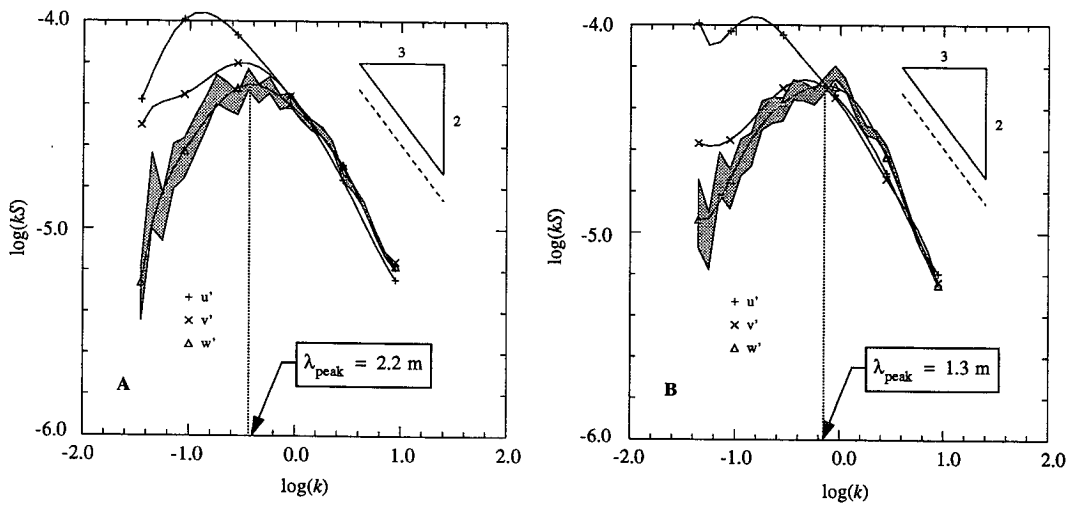


FIG. 6. Six-hour average spectra 7 m below the ice in the same representation as Fig. 1, before and after crossing the temperature front (indicated by arrows in Fig. 5).

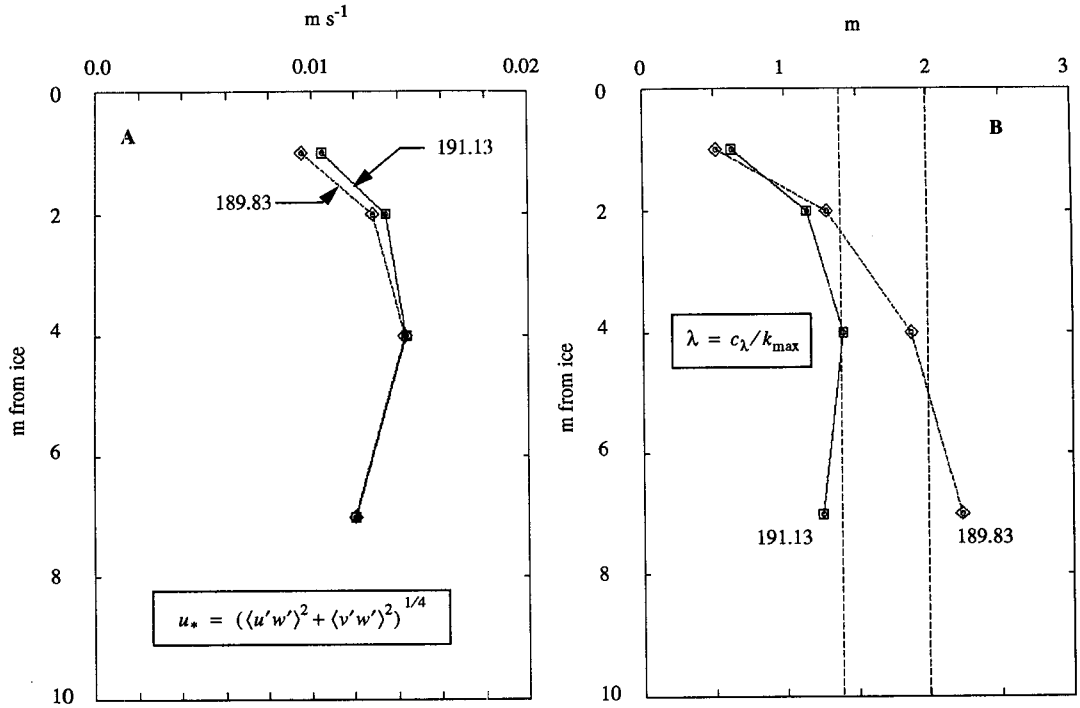


FIG. 7. Comparison of friction velocity (a) and turbulent mixing length (b) in the MIZEX 84 mixed layer for 6-h averages before and after crossing the thermal front.

copter to the edge of a nearby active lead (a lead is a substantial crack in sea ice; it is active when open water or very thin ice is in contact with cold air) in order to gauge the effect of rapid freezing on the atmospheric and oceanic boundary layers (LEADEX Group 1993).

One component of the lead instrumentation was a mast on which four TICs were mounted spanning 6 m, so that Clusters 2, 3, and 4 were mounted 1, 3, and 6 m, respectively, below the topmost Cluster 1. The mast, equipped with a vane for maintaining orientation into the mean flow, could be lowered as a rigid unit to any level in the upper 50 m. Its direction, depth, and vertical alignment were measured with flux-gate compass, pressure gauge, and tiltmeters, respectively. It was typically deployed either over the edge of the lead or through a hole in the ice about 3 m back from the edge. For Cluster 2, a SeaBird SBE-07 microstructure conductivity ($\mu$C) meter replaced the standard SeaBird SBE-04 conductivity meter. During the deployments, output from the $\mu$C sensor drifted approximately linearly away from a standard calibration value, but when this linear trend was removed, low-frequency excursions agreed well with those seen in the adjacent standard conductivity meters. Salinity variance spectra, calculated using the $\mu$C output, were similar in shape to temperature spectra, and exhibited a well-developed inertial subrange. The $\mu$C-equipped TIC was used to calculate salinity flux, $\langle w'S' \rangle$, directly. As far as we know, these are the first direct salinity flux measurements made in a natural oceanic flow.

At the third lead deployment (Lead 3), conditions were nearly ideal for the TIC mast. The temporary station, sited at the north edge of a kilometer-wide lead, drifted south for the better part of a day at about 13 cm $s^{-1}$ in response to a moderate northerly breeze. Currents measured relative to the drifting floe (Fig. 10) came from almost directly across the lead, representative of conditions in fluid that had traversed its entire width. The true bearing of the lead edge measured in front of the TIC mast was approximately 82 deg. In a frame of reference fixed to the drifting ice (our measurement frame) the mean relative current velocity perpendicular to the ice edge was about 11 cm $s^{-1}$, with a transit time across the lead on the order of 3 h. The currents were relatively steady until they slowed abruptly shortly after 99.0 [which was about 3 h after local noon on day 98—see LEADEX Group (1993), their Fig. 3]. In the first part of the period, the mast was positioned in the upper 10 m of the water column; later it was lowered to about halfway through the mixed layer.

Averaged vertical velocity spectra are shown for each cluster on the mast during the shallow and middepth deployments in Fig. 11. Except at 3.3-m depth, the spectral peaks have shifted to significantly lower wavenumbers compared with previous examples, and even at that level there is a broad plateau spanning about a decade of wavenumber scale. These plateaus at shallower depths result from averaging highly variable, individual 1-h spectra. We interpret this variability as a

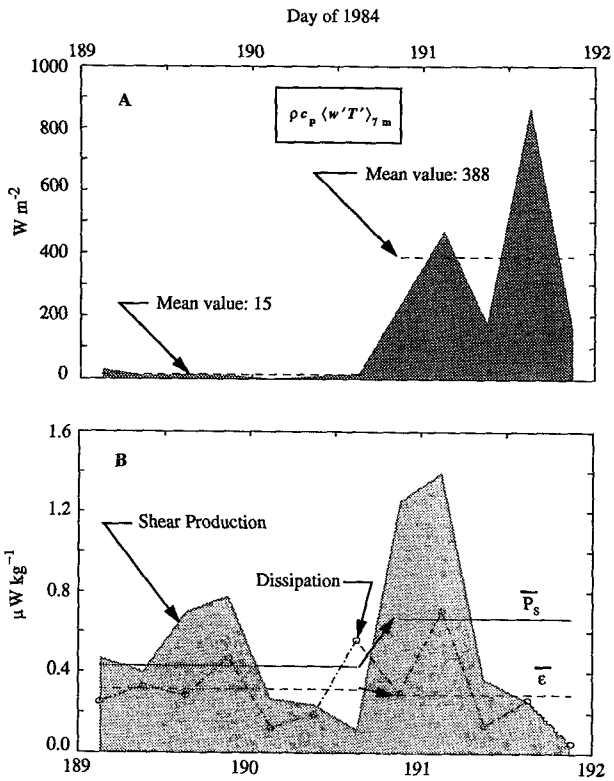


FIG. 8. Summary of turbulent energetics 7 m below the ice during the MIZEX 84 storm. (a) Six-hour average turbulent heat flux (shaded curve). Mean values before and after crossing the thermal front are indicated by the dashed horizons. (b) TKE shear production (shaded curve) and dissipation (circles connected by dot–dash curve). Mean values before and after crossing the front are indicated by solid (production) and dashed (dissipation) lines.

competition between the normal scales of shear-driven turbulence (near zero on the log$k$ axis) and a scale associated with more highly organized convective features that persist throughout the mixed layer (with a peak near $-1$ on the log$k$ axis). Turbulent mixing length scales were calculated from the peaks in the hourly $w$ spectra as before (Fig. 12). When the mast was shallow, there was much variability, both vertical and temporal. Note that for Clusters 2 and 3, particularly, there is a tendency to swing from short scales to long as the shear scale or organized convection scale dominates the hourly averages. After the mast was lowered to the 14–20 m range, $\lambda$ is relatively consistent across the mast, suggesting that the large turbulent features are coherent over a vertical span of at least 6 m, and probably across most of the mixed layer. At 9.3 m and deeper, the large-scale features control the spectra, and the maximum mixing length is relatively uniform.

For the time when the mast was shallow, surface friction velocity, $u_{*0}$, and buoyancy flux, $\langle w'b' \rangle_0$ (11), were estimated from the measured Reynolds stress at 3.3 m (Cluster 1) and the measured salinity and heat flux at 4.3 m (Cluster 2), assuming that turbulent fluxes at those levels represented surface conditions. The data are summarized in Fig. 13. Each symbol represents a 1-h average every half hour when the TIC mast was operating. Although $\langle w'T' \rangle_{4.3\,m}$ (not shown) was measured and used in the buoyancy flux calculation, it turned out to have negligible effect. The main distinguishing feature of the flux measurements is the persistent salt flux from freezing at the surface of the lead. Obukhov length, $L_0 = u_{*0}^3/\kappa\langle w'b' \rangle_0$, based on the near-surface flux measurements, is shown in the bottom panel. Here, $L_0$ varies more from changes in friction velocity than buoyancy flux.

Mean values for $\lambda$ based on the spectral peaks are plotted versus depth in Fig. 14. Of six hourly samples obtained after lowering the mast to midway in the mixed layer, the averages of the first three (between 98.75 and 98.85) are plotted, because during that time the salinity flux was about half the previous value measured near the surface. We have found from numerical modeling that as a first-order approximation, salinity flux falls off linearly from the surface to the pycnocline; thus, we assume that the surface flux was not much different from earlier. After 98.85, $\langle w'S' \rangle_{14.8\,m}$ was about 1/5 its previous value, as midday solar heating decreased freezing. The premise is that although the circled measurements at middepth in the mixed layer were not simultaneous with the shallow measurements, they represent roughly similar conditions of surface forcing.

Figure 14 suggests a paradigm for the distribution of $\lambda$ in the convecting (statically unstable) mixed layer as follows. In the surface layer $\lambda$ increases much more rapidly with depth than neutral $\kappa|z|$ scaling, until reaching a maximum value of about $\lambda_{max} = \kappa|z_{ml}|$. For greater depths, it retains this value, which is set by the largest organized convective eddies in the mixed layer. The rate at which $\lambda$ increases with depth depends on $L_0$, that is, on surface friction velocity and buoyancy flux. Using the mean value of Obukhov length when the frame was shallow, $L_0 = -12.1$ m, three possibilities for this dependence are shown in Fig. 14. With $\zeta = |z|/L_0$, the curve labeled "Businger–Dyer" (Businger et al. 1971) is

$$\lambda = \kappa|z|(1 - 15\zeta)^{1/4}, \qquad (13)$$

while the other two curves are from a simplified version

$$\lambda = \kappa|z|(1 - \zeta)^n \qquad (14)$$

for $n = 1$ and 2. At these scales there is little difference between (13) and (14) with $n = 1$, but the data fall closer to (14) with $n = 2$. Error bars indicate large variability in the upper few meters, and it might be argued that the Businger–Dyer formula, obtained from an extensive observational base, is more appropriate. In this regard, however, it should be noted that because of the disparity in scales between the atmospheric and oceanic boundary layers, atmospheric measurements

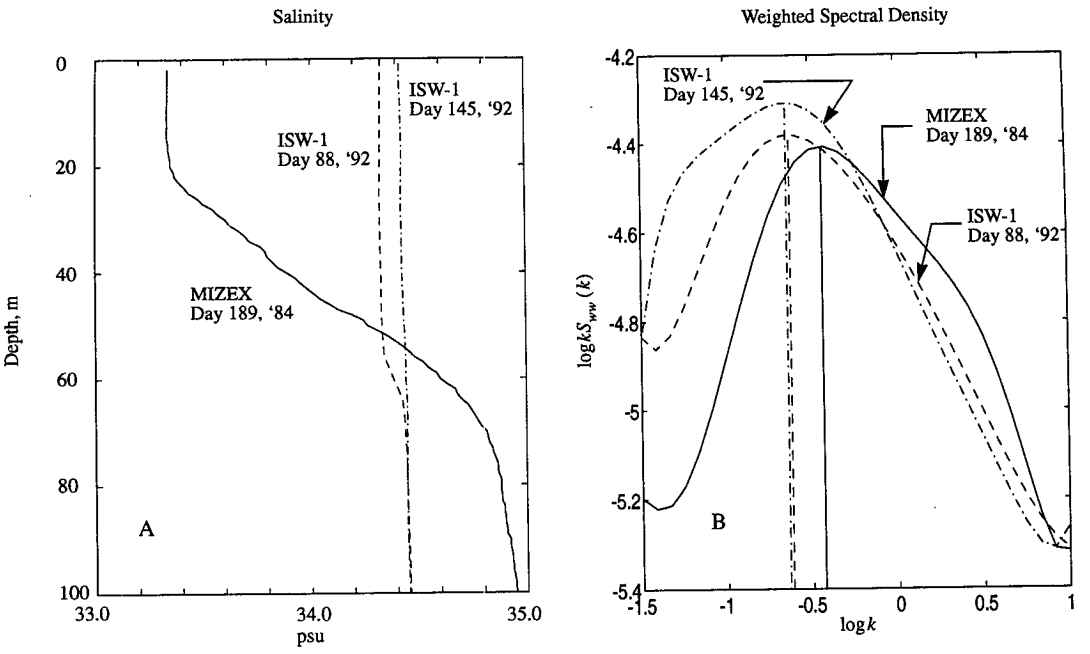


FIG. 9. Comparison of vertical velocity spectra under similar conditions of Reynolds stress but variable mixed layer depth. (a) Salinity profiles from MIZEX 84, day 189 (courtesy J. Morison), and from ISW-1 during storms on days 88 and 145 (courtesy B. Huber and A. Gordon). By day 145 (24 May) the seasonal pycnocline had practically disappeared. (b) Weighted vertical velocity spectra for 6-h averages near the time of the CTD casts. The spectra labeled "ISW-1" are from a TIC mounted 16 m below the ice (to ensure no surface-layer effect). The one labeled "MIZEX" is from 7 m below the ice.

from a similar regime are not common. Consider, for example, our measurements at 6.3 m for which $\zeta \approx -0.5$. Assuming 30:1 scaling, in a *similar* atmosphere, the measurement level would be 200 m, and the nondimensional coordinate at the standard 10-m meteorological level would be $\zeta \approx -0.02$.

## 3. Mixing length formulation

### a. *Mixing length in the mixed layer and upper pycnocline*

Following earlier work (McPhee 1981, 1987, 1990) we posit that for the neutral or stably stratified boundary layer, the mixing length increases linearly with increasing distance from the surface until it reaches a maximum value, $\lambda_{max}$. If $\langle w'b' \rangle_0$ vanishes (neutral stability) the maximum is proportional to the planetary length scale:

$$\lambda_{max} = \Lambda_* u_{*0} / |f_{cor}|; \quad L_0 \to \pm\infty \quad \text{(neutral)}, \quad (15)$$

where the numerical value for the constant, $\Lambda_*$, determined from the ISW-1 data (McPhee and Martinson 1994) is about 0.028. In a highly stable boundary layer (Businger and Arya 1974; Zilitinkevich 1975)

$$\lambda_{max} = \kappa R_c L_0; \quad L_0 \to 0^+ \quad \text{(highly stable)}, \quad (16)$$

where $R_c$ is the critical flux Richardson number (a constant with numerical value about 0.2). An expression satisfying these limits is

$$\lambda_{max} = \Lambda_* u_{*0} \eta_*^2 / |f_{cor}| \quad \text{(neutral or stable)}, \quad (17)$$

where $\eta_*$ is a stability factor (McPhee 1981)

$$\eta_* = \left(1 + \frac{\Lambda_* u_{*0}}{\kappa |f_{cor}|} \frac{1}{R_c L_0}\right)^{-1/2}. \quad (18)$$

An algorithm for calculating $\lambda$ in the mixed layer is presented as a flow chart in Fig. 15. It combines (17) with the development for the unstable PBL in section 2c, using (14) in the surface layer, with $n = 2$.

For depths greater than the mixed layer depth (typically defined by the level at which the mean buoyancy frequency exceeds a specified threshold), we assume that $\lambda_{pyc} = \kappa R_c L$, where $L$ is the *local* Obukhov length, derived from the local Reynolds stress and buoyancy flux. This acknowledges that the scale of turbulence in the pycnocline is fundamentally different from the scale of "free" eddies in the well-mixed layer.

It should be noted that $\lambda$ is not directly comparable to the *master turbulent length* scale of the Mellor and Yamada (1982) second-moment turbulence closure scheme. In their "level 2½" version, for example, the master turbulent length scale, $l$, is obtained from a prognostic equation for the product of $l$ and twice the

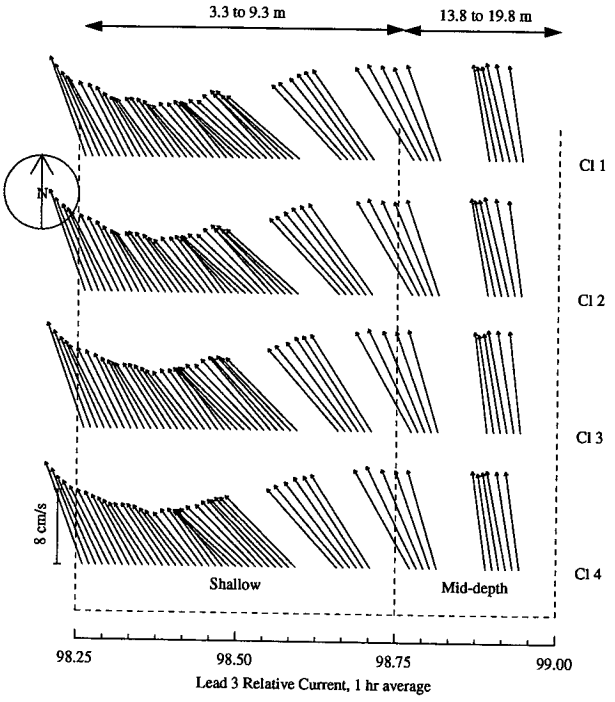


FIG. 10. Mean current relative to the TIC mast located at the north edge of an east–west aligned lead. During this time, the ice and lead were drifting south at about 13 cm $s^{-1}$. For the first part of the period, the mast was positioned with TICs at 3.3, 4.3, 6.3, and 9.3 m. Later it was lowered as a unit to span depths 13.8 to 19.8 m. The mixed layer during this time was between 28 and 30 m deep. The mast was deployed about 3 m from the edge of the lead, through a hole in 1.3-m ice.

TKE per unit mass. Stability effects are incorporated into the eddy diffusivity coefficients by means of separate stability factors. A mixing length comparable to $\lambda$ may be derived from the Mellor–Yamada solutions by dividing the eddy viscosity by the square root of the local stress magnitude.

### *b. Demonstration with a simple numerical model*

A hypothetical simulation, which may bear some similarity to actual conditions in the central and eastern Weddell Sea, illustrates the mixing length formulation developed here. The region poses a conundrum in that it appears to support a high (by polar standards) heat flux up through the mixed layer that significantly inhibits ice growth during winter (Gordon and Huber 1990), yet if the ice underwent much additional growth (in some areas a few tens of centimeters), salt added to the water column would cause it to become statically unstable and convect to great depth, with much greater heat loss to the atmosphere (Martinson 1990). Depending on a delicate balance among thermal expansion, melting, and ice export, once the process started, the region might go into a quasi-permanent mode of deep convection that would greatly increase cooling and ventilation of the deep ocean (Martinson 1991). The Weddell Polynya of the mid-1970s (Zwally and Gloersen 1977) was an area comprising about 10% of the Weddell Sea that remained ice free for several winters in a region normally covered by seasonal sea ice. It is thought to be an example of an unstable mode in which deep convection reigned (Martinson et al. 1981) with significant impact on deep-water formation (Gordon 1982).

One of the more puzzling aspects of Weddell air–sea–ice interaction is the apparent combination of a deep, well-mixed layer with large heat flux from below. From various lines of reasoning, Gordon and Huber (1990) estimated that in the so-called "warm regime" of the Weddell (maximum temperature in the water column of order 1°C), the heat flux through the mixed layer and ice cover to the air averages between 30 and 40 W $m^{-2}$ during winter. At high latitudes, Coriolis attenuation of the turbulent stress is strong, and processes that would diffuse or advect heat upward through the pycnocline would also tend to shallow the mixed layer. The lack of much ice growth after a few weeks early in the winter (Martinson 1990) precludes unstable buoyancy flux through much of the season (since sensible heat flux has negligible impact on buoyancy flux at temperatures near freezing). The question then is how shear at the surface provides enough turbulence to drive the intense mixing at depth. Drifting buoys (Baker and Martinson 1990) have shown that storms with peak surface winds of 25–35 m $s^{-1}$ are not uncommon in the central and eastern Weddell. In preparing for a planned project to measure wintertime fluxes in the eastern Weddell, we investigated the role these storms might play in maintaining the high heat flux and deep mixed layers, using a simple numerical model based on the present mixing length (first-order closure) scheme.

Two idealized scenarios were compared, each integrated for 20 days. Both are started from observed warm-regime temperature and salinity profiles (Huber et al. 1989; their CTD cast number 18), except that the mixed layer, which was measured to be about 0.05°C above freezing, is set initially to its freezing temperature. In each case, a constant heat flux of 34 W $m^{-2}$ is conducted through the ice to the atmosphere. The initial ice thickness is 1 m. The two simulations differ in their treatment of stress at the ice–ocean interface. In the "storm scenario," the momentum flux is concentrated in two storm events spaced 10 days apart. The maximum friction velocity is $u_{*0}$ = 0.04 m $s^{-1}$, which implies a peak wind of about 30 m $s^{-1}$, given a typical 10-m wind drag coefficient for the Weddell (Wamser and Martinson 1993) and no internal ice force. In the other case, the stress is constant (after a 1-day start-up ramp) with the same mean value as the storm scenario. Prescribed values for $u_{*0}$ are graphed in Fig. 16a. Note that the mean value of $u_{*0}$ in each case implies an average wind of about 11 m $s^{-1}$.

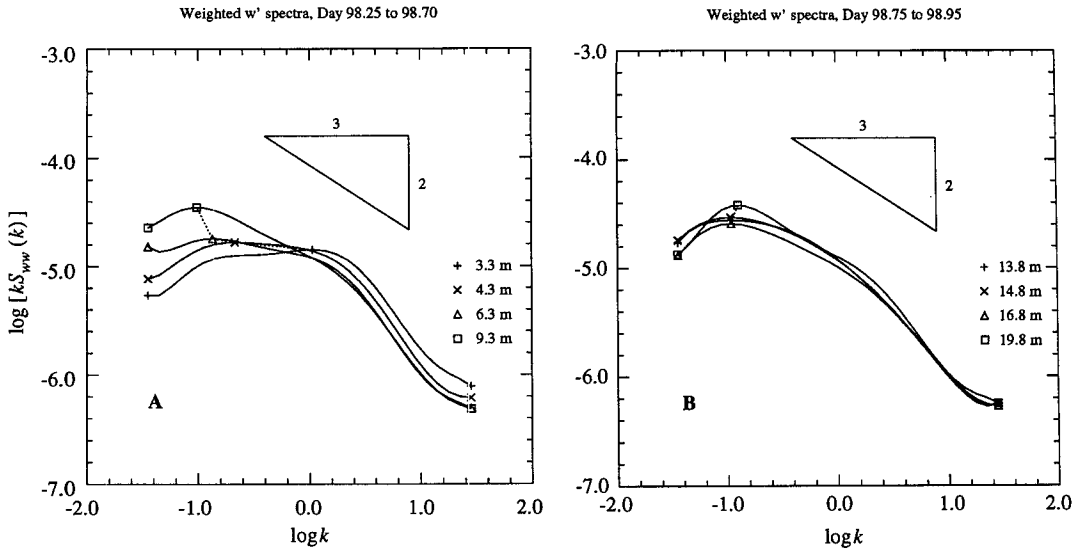


FIG. 11. Weighted vertical velocity spectra averaged over the period when the TIC mast was shallow (a) and middepth in the mixed layer (b). Note the "plateaus" at shallower depths, indicating competition between shear-driven eddies and larger-scale organized features resulting from brine-driven convection.

The equations solved are

$$\hat{u}_t + if_{\text{cor}}\hat{u} + \underline{w}\hat{u}_z = (-K\hat{u}_z)_z$$
$$S_t + \underline{w}S_z = (-\alpha K S_z)_z$$
$$T_t + \underline{w}T_z = (-\alpha K T_z)_z, \qquad (19)$$

where subscripts denote partial differentiation, $\hat{u} = u + iv$ is the complex horizontal velocity, and $\underline{w}$ is a prescribed upwelling velocity. We use a right-handed coordinate system with $z$ upward, and $K = \lambda u_*$ is the eddy viscosity, where $\lambda$ is the mixing length from section 3a and $u_*$ is the local friction velocity. In the mixed layer proper with small gradient Richardson number

$$\text{Ri} = \left(-\frac{g}{\rho}\frac{\partial \rho}{\partial z}\right) \Big/ |\hat{u}_z|^2,$$

scalar eddy diffusivity and eddy viscosity are taken to be equal. In the underlying pycnocline, where internal waves often play a role in initiating and maintaining turbulence and can be more effective at transporting momentum than properties like heat and salt, the diffusivities may differ appreciably. In the model, the ratio of scalar eddy diffusivity to eddy viscosity is given by

$$\alpha = \begin{cases} 1, & \text{Ri} \leqslant 0.79 \\ e^{-1.5\sqrt{(\text{Ri} - 0.079)}}, & 0.79 < \text{Ri} < 5 \\ 0.039, & \text{Ri} > 5 \end{cases}, \qquad (20)$$

which provides an efficient approximation to the dependence of $\alpha$ on Ri suggested by Turner (1973, chapter 5). These simulations were done with $\underline{w}$ equal to zero, and background diffusivities in the nonturbulent pycnocline set to their molecular values.

Boundary conditions are supplied from the prescribed friction velocity (see Fig. 16a) and a simplified ice–ocean heat flux model (McPhee 1992):

$$\langle w'T' \rangle_0 = u_{*0} c_h [T_{\text{ml}} - T_f(S_{\text{ml}})]$$
$$\langle w'S' \rangle_0 = \frac{S_{\text{ml}} - S_{\text{ice}}}{Q_L} (\langle w'T' \rangle_0 - \dot{q}), \qquad (21)$$

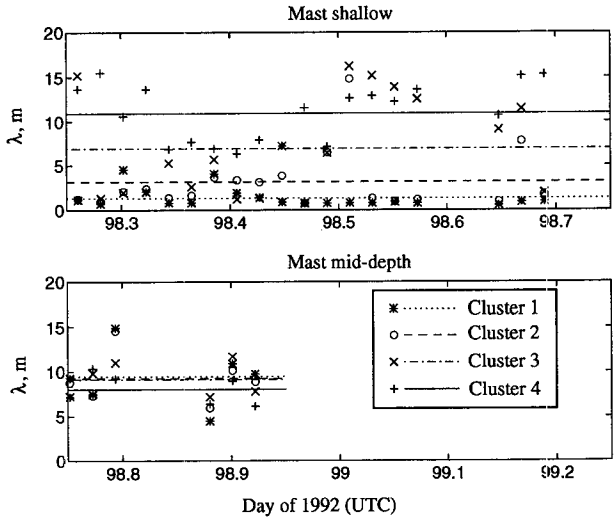


FIG. 12. Mixing length based on the peaks in the $w$ spectra calculated from hourly time series every half hour (symbols, see key) for the periods when the mast was shallow (upper panel) and middepth (lower). The lines represent averages in each period. During the shallow period, there is much variability at Clusters 2 (4.3 m) and 3 (6.3 m) depending on whether the large-scale features (with typical timescales ~10 min) or shear-driven eddies (typical time scales, 2–3 min) dominate the 1-h spectra.

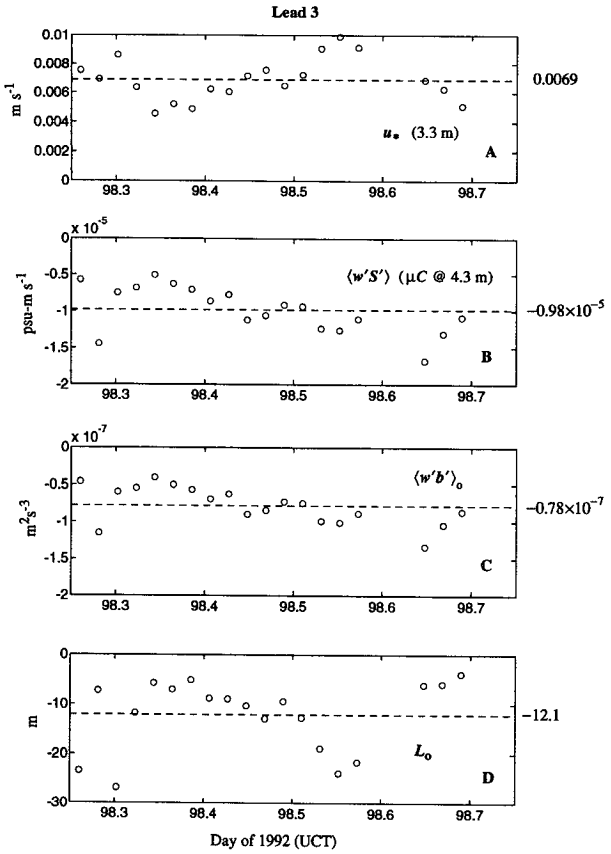


FIG. 13. Time series of (a) friction velocity at 3.3 m; (b) salinity flux at 4.3 m; (c) buoyancy flux, from the salinity flux and turbulent heat flux, at 4.3 m; and (d) the surface Obhukov length, calculated assuming the friction velocity and buoyancy flux are representative of surface conditions. Dashed horizons are the mean values, with magnitudes listed at right.

where $T_{ml}$ is mixed layer temperature, $T_f(S_{ml})$ is the mixed layer freezing temperature, $\dot{q}$ is heat flux conducted through the ice divided by the product of density and specific heat for sea water, and $c_h = 0.006$ is the heat transfer coefficient.

Concentrating the momentum flux into storm events has a markedly nonlinear response in the model. Heat flux at the ice–ocean interface is significantly enhanced in the storm scenario (Fig. 16b), with a mean value about five times as large as for the steady wind: 34.4 versus 6.9 W m$^{-2}$. Salinity flux also differs (Fig. 16c) with the large heat flux events accompanied by ice melting. The steady case exhibits persistent negative salinity flux (freezing), but mean salinity flux in the storm simulation is about zero, as confirmed by the ice draft (Fig. 16d). Whereas there is essentially no ice growth over the 20-day storm simulation, the steady-wind ice cover grows by about 20 cm. In some parts of the Weddell Sea, the salt flux associated with this growth difference is a significant fraction of that needed to destabilize the upper ocean.

The episodic nature of heat flux throughout the mixed layer and upper pycnocline is demonstrated in Fig. 17. The modeling implies that even though the peak friction velocity (wind) is less than three times the steady value, heat flux near the base of the mixed layer can be 25 times as intense. During a storm, this heat is partitioned into (i) warming the mixed layer, (ii) melting ice, and (iii) conduction through the ice to the atmosphere. The agent for high turbulent heat flux is much enhanced eddy viscosity (Fig. 18). The maximum value of $K$ in the mixed layer during a storm is 0.277 m$^2$ s$^{-1}$ versus 0.044 for the steady case.

The idealized forcing in this comparison is somewhat artificial: it is unlikely, for example, that heat flux out of the ice–ocean system would remain constant during high winds (although increased wind turbulence might be offset to some degree by warmer air temperatures during the storms, which typically migrate from the north). Still, the very simple numerical model provides a plausible explanation for the large heat flux values inferred for the central and eastern Weddell Sea, suggesting that the nature of the distribution of wind stress (e.g., intense storms) is at least as important as its mean value.

## 4. Summary

The primary object of this paper is to present a concise algorithm for estimating the turbulent mixing

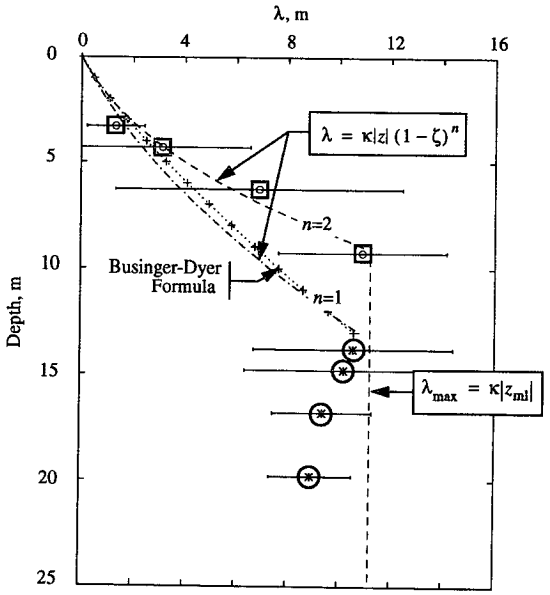


FIG. 14. Profiles of average mixing length from spectral peaks, when the mast was shallow (square symbols) and middepth (circles). Error bars are twice the sample standard deviation. Three surface-layer formulas, based mean values of $u_{*0}$ and $L_0$ from Fig. 13, are shown: the Businger–Dyer formula (pluses connected by dots), and a simpler formula (see text) with $n = 1$ (dot–dash) and $n = 2$ (dashed). A limit based on the mixed layer depth is shown as the vertical dashed line.

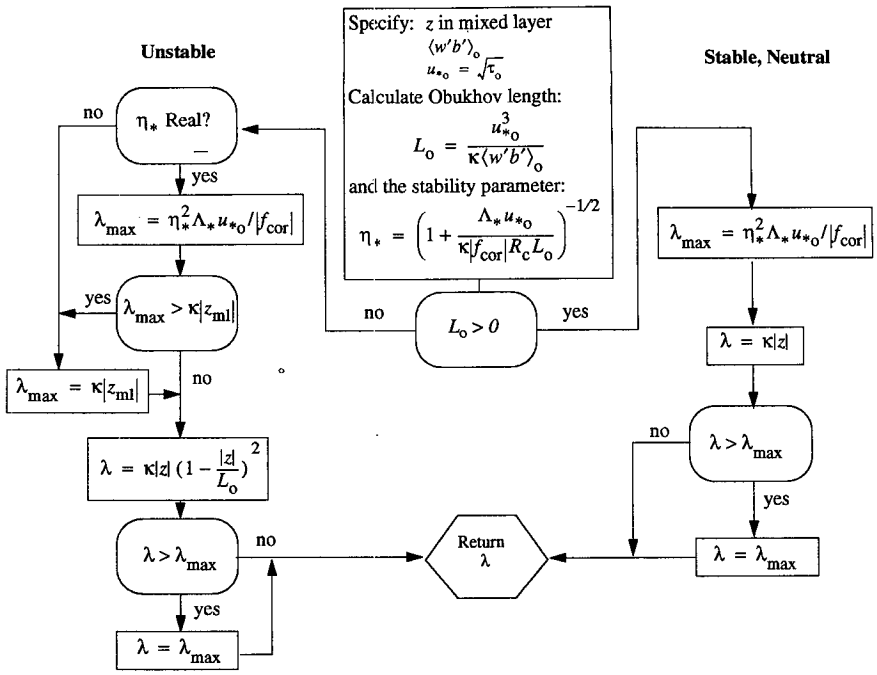


FIG. 15. Flowchart describing the computation of mixing length in the well-mixed layer, given vertical displacement, surface (interface) friction velocity, and surface buoyancy flux. Values suggested for the dimensionless constants are $R_c = 0.2$ and $\Lambda_* = 0.028$. This does not hold for the pycnocline below the mixed layer.

length in the oceanic mixed layer. From that perspective, the main result is the flow chart of Fig. 15. The work is mostly consistent with earlier formulations of a similarity theory (McPhee 1981, 1983) and numerical model for the upper ocean (McPhee 1987) based on under-ice flux measurements, but extends the analysis by (i) developing and using a direct measure of the mixing length, $\lambda$, based on the peak in the weighted wavenumber spectrum of vertical velocity variance; and (ii) using the first direct measurements of total buoyancy flux (i.e., $\langle w'T' \rangle$ and $\langle w'S' \rangle$) to formulate a realistic $\lambda$ distribution for a statically unstable, convecting oceanic boundary layer.

The concept of using the $w$ spectral peak as an empirical method for estimating $\lambda$ is an important subtheme of the paper. It derives from work on atmospheric surface-layer vertical wind spectra of Busch and Panofsky (1968), who showed that the wavelength at the peak in the weighted spectrum scaled with distance from the surface; as does $\lambda$ for the neutral surface layer. For measurement levels outside the surface layer, comprising most oceanic measurements, $\lambda$ loses its $z$ dependence, but the contention is that it retains its proportionality to peak wavelength (McPhee and Smith 1976). Under-ice turbulence and spectra data in section 2, and also reported by McPhee and Martinson (1994), support the hypothesis. There are good reasons for developing this tool. First, it provides a direct means of estimating eddy viscosity locally, without having to also measure the mean gradient. In the oceanic mixed layer, mean gradients associated with turbulent fluxes are so small that it is sometimes a more daunting task to measure them than it is to measure the turbulent covariance statistics directly. Being able to measure vertical distributions of eddy viscosity provides a powerful and useful constraint on theoretical/numerical modeling activities. Second, the technique provides the necessary length scale for using spectra of vertical velocity and temperature to estimate flux magnitudes by the inertial–dissipation method (Fig. 4). In general, it is simpler to measure meaningful spectra into the inertial subrange than it is the three-dimensional velocity field needed for direct covariance measurements, especially in the presence of mooring or platform motion. As our turbulence database expands, it may also be possible to ascertain the Kolmogorov constant for salinity variance dissipation by comparing salinity variance spectra with $\langle w'S' \rangle$ measurements made using microconductivity sensors.

A valid question regarding this work is how applicable it is to the open ocean mixed layer, where surface waves (instead of pack ice) are a significant intermediary in the transfer of momentum from the air to the ocean. In theory, surface wave interactions can produce organized eddies in the neutral or stable open ocean boundary layer (Liebovich and Paolucci 1980) that may be more efficient at transporting momentum and scalar properties than the shear-driven eddies of wall-

bounded flows. The impact of these rolls would be somewhat analogous to the organized convective structures observed under moderately unstable conditions at Lead 3 (section 2c): they might increase the effective mixing length, perhaps also to something like $\kappa|z_{ml}|$. The overall effect would be to increase the eddy viscosity, in which case our neutral results would serve as a lower bound. It may be that a good gauge of the relative importance of Langmuir circulations in upper ocean mixing is the degree to which they dominate the vertical velocity spectra in a particular flow. Results of section 3b suggest that a disproportionate amount of mixing occurs in extreme storm events. The maximum eddy viscosity scales with $u_{*0}^2$, which is essentially proportional to the square of the wind speed. To show that Langmuir cells or other secondary circulations dominate mixing in high winds, one would have to show that the mixing strength of the circulations has at least quadratic dependence on wind speed.

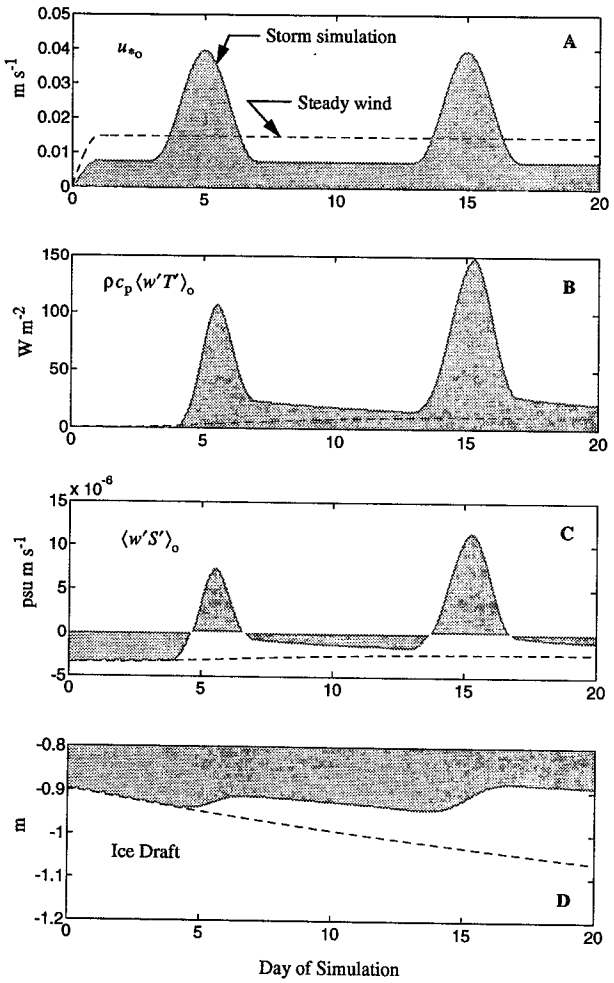


FIG. 16. Ice–ocean interface conditions for model demonstration. In each case, the shaded curve refers to the "Storm Scenario" and the dashed curve to the "Steady Scenario." (a) Prescribed friction velocity (square root of kinematic boundary stress). Mean values are the same. (b) Oceanic heat flux. (c) Salinity flux. (d) Ice draft ($\rho_{ice}h_{ice}/\rho_w$).

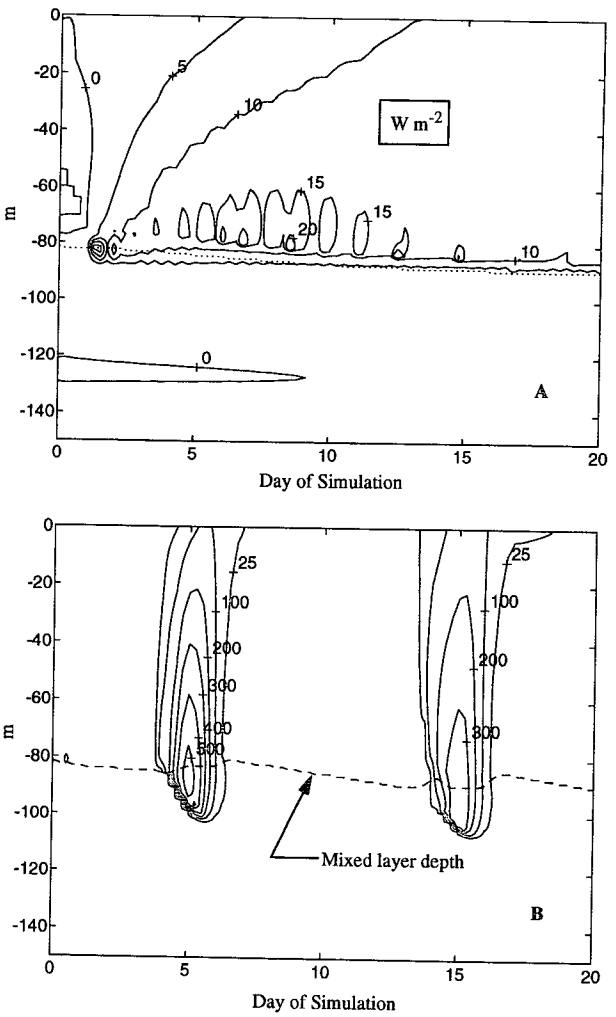


FIG. 17. Contour plots of turbulent heat flux in the upper ocean, for the "Steady Scenario" (a) and the "Storm Scenario" (b).

During LEADEX, eddy viscosity values as high as 0.06 $m^2 s^{-1}$ were measured with moderately low surface stress, and simulated Weddell Sea storms implied eddy viscosities as high as 0.2 $m^2 s^{-1}$. The latter is at least an order of magnitude greater than parameterizations for the neutral eddy viscosity commonly used in three-dimensional ocean models (Smith and Hess 1993).[2] The modeled turbulence is generated almost entirely by shear stress at the surface; thus, its gross features are described with simple Rossby similarity theory.

[2] This is not true, however, of the Mellor–Yamada level 2½ second-moment closure model. Parallel simulations of the scenarios described in section 3b with MY 2½ led to generally similar results: for example, mean values of oceanic heat flux at the ice–ocean interface were 34 and 12 W $m^2$ for the storm and steady scenarios, respectively, compared with 34 and 7 W $m^2$ using the present model.

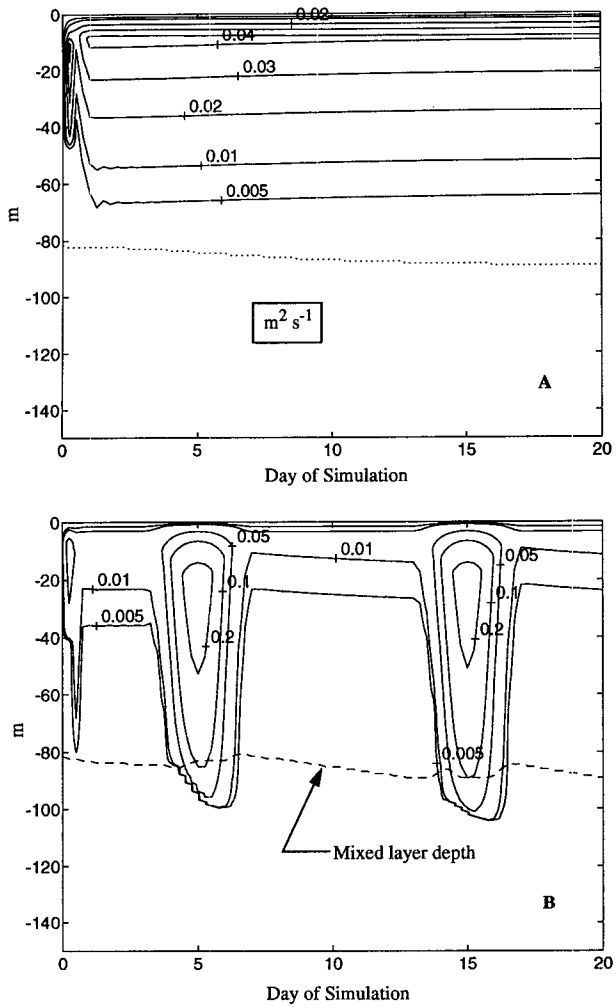


FIG. 18. Contour plots of eddy viscosity in the upper ocean, for the "Steady Scenario" (a) and the "Storm Scenario" (b).

Section 1 stressed the exploratory nature of this paper. Over the past several years we have accumulated a fairly large database on upper ocean turbulence under drifting ice stations, and data discussed in this work are only a small fraction of the total. It is possible to find examples that do not conform with the principles outlined here. A notable one is from the 1989 Coordinated Eastern Arctic Experiment (CEAREX) north of Fram Strait. Eddy viscosities as high as 0.15 $m^2 s^{-1}$ were observed when the friction velocity was between 0.01 and 0.014 m $s^{-1}$ (see McPhee 1992, Fig. 16). This implies mixing lengths of 10 m or more, despite the fact that the surrounding ice was thick enough to prevent any appreciable surface buoyancy flux. The regime was different from those described here, in that the primary source of shear at the ice/ocean boundary was from diurnal tidal currents, apparently associated with circulation about the Yermak Plateau (Padman et al. 1992), rather than wind-driven ice drift. The internal wave field below the mixed layer was also anomalously active, including regular appearance of an energetic bore in the pycnocline. Based on upward attenuation of energy in the internal wave band observed when a TIC frame spanned the mixed layer–pycnocline interface, we speculated (McPhee 1991) that internal waves impinging on the mixed layer from below added significantly to its turbulent kinetic energy, increasing the turbulence scales in a way analogous to unstable buoyancy flux.

In a thoughtful acceptance of the Roger Revelle Award, Lorenz (1993) admonished against selectively presenting data from potentially chaotic systems that support whatever principle or model one has in mind, when there are other data that do not. The CEAREX 89 data do not fit the present model, but a separate physical forcing mechanism not considered in this development appears to have been responsible. It seems likely that if we returned to Fram Strait under similar conditions, we would find a similar boundary layer with anomalously large mixing lengths. In other words, at these scales the response of the boundary layer is probably not chaotic, yet the possibility remains and should be entertained.

*Acknowledgments.* Polar field experimentation is almost always a very cooperative venture, and the work described here owes much to a large number of people. Of the two most recent programs (LEADEX and ISW-1), neither would have been possible without the direct assistance of Roger Andersen, Ted Baker, Tom Lehman, and Doug Martinson. My perception of how turbulent boundary layers work has been influenced especially by exchange of ideas with Lakshmi Kantha, Doug Martinson, George Mellor, Jamie Morison, and J. D. Smith. None of this would have happened without long term support from G. Leonard Johnson and Tom Curtin of the Office of Naval Research. The work was funded by the Office of Naval Research under Contract N00014-84-C-0028 and by the National Science Foundation Office of Polar Programs under Grants OPP-9110422 and DPP-9210134.

## REFERENCES

Baker, T. N., and D. G. Martinson, 1990: Antarctic oceanographic/meteorological SALARGOS buoy data: March 1988–June 1989. Tech. Rep. LDGO-90-1, Lamont–Doherty Geological Observatory, Palisades, NY 10964, 163 pp.

Bloomfield, P., 1976: *Fourier Analysis of Time Series: An Introduction.* John Wiley and Sons, 258 pp.

Busch, N. E., and H. A. Panofsky, 1968: Recent spectra of atmospheric turbulence. *Quart. J. Roy. Meteor. Soc.*, **94,** 132–147.

Businger, J. A., and S. P. S. Arya, 1974: The height of the mixed layer in the stably stratified planetary boundary layer. *Advances in Geophysics,* Vol. 18A, Academic Press, 73–92.

——, J. C. Wyngaard, Y. Izumi, and E. F. Bradley, 1971: Flux-profile relationships in the atmospheric surface layer. *J. Atmos. Sci.*, **28,** 181–189.

Dillon, T. M., 1982: Vertical overturns: A comparison of Thorpe and Osmidov length scales. *J. Geophys. Res.*, **87,** 9601–9603.

Edson, J. B., C. W. Fairall, P. G. Mestayer, and S. E. Larsen, 1991: A study of the inertial-dissipation method for computing air–sea fluxes. *J. Geophys. Res.*, **96,** 10 689–10 711.

Gargett, A., 1990: Do we really know how to scale the turbulent kinetic energy dissipation rate $\varepsilon$ due to breaking of oceanic internal waves? *J. Geophys. Res.*, **95,** 15 971–15 974.

Gordon, A. L., 1982: Weddell deep water variability. *J. Mar. Res.*, **40,** 199–217.

——, and B. A. Huber, 1990: Southern Ocean winter mixed layer. *J. Geophys. Res.*, **95,** 11 655–11 672.

Gregg, M. C., 1987: Diapycnal mixing in the thermocline: A review. *J. Geophys. Res.*, **92,** 5249–5286.

Gross, T. F., and A. R. M. Nowell, 1985: Spectra scaling in a tidal boundary layer. *J. Phys. Oceanogr.*, **15,** 496–508.

Hinze, J. O., 1975: *Turbulence.* 2d ed. McGraw-Hill, 790 pp.

Hopfinger, E. J., 1987: Turbulence in stratified fluids: A review. *J. Geophys. Res.*, **92,** 5287–5303.

Huber, B. A., P. A. Mele, W. E. Haines, A. L. Gordon, J. C. Jennings, L. I. Gordon, R. F. Weiss, F. A. Van Woy, and P. K. Salameh, 1989: CTD and hydrographic data from Cruise ANT V/2 of R/V *Polarstern,* Tech. Rep. LDGO-89-3, 245 pp. [Available from Lamont–Doherty Geological Observatory, Palisades, NY 10964.]

ISW Group, 1993: Weddell Sea exploration from ice station. *Eos, Trans. Amer. Geophys. Union,* **74,** 112 pp.

Kraus, E. B., and J. S. Turner, 1967: A one-dimensional model of the seasonal thermocline: II. The general theory and its consequences. *Tellus,* **19,** 98–106.

Langleben, M. P., 1982: Water drag coefficient of first-year sea ice. *J. Geophys. Res.*, **87,** 573–578.

LEADEX Group, 1993: The LEADEX Experiment. *Eos, Trans. Amer. Geophys. Union,* **74,** 393 pp.

Liebovich, S., and S. Paolucci, 1980: The Langmuir circulation instability as a mixing mechanism in the upper ocean. *J. Phys. Oceanogr.*, **10,** 186–207.

Lorenz, E. N., 1993: Response. *Eos, Trans. Amer. Geophys. Union,* **74,** 301.

Martinson, D. G., 1990: Evolution of the Southern Ocean winter mixed layer and sea ice: Open ocean deepwater formation and ventilation. *J. Geophys. Res.*, **95,** 11 641–11 654.

——, 1991: Open ocean convection in the Southern Ocean. *Deep Convection and Deep Water Formation in the Oceans,* P.-C. Chu and J.-C. Gascard, Eds., Elsevier, 37–52.

McPhee, M. G., 1981: An analytic similarity theory for the planetary boundary layer stabilized by surface buoyancy. *Bound.-Layer Meteor.*, **21,** 325–339.

——, 1983: Turbulent heat and momentum transfer in the oceanic boundary layer under melting pack ice. *J. Geophys. Res.*, **88,** 2827–2835.

——, 1987: A time-dependent model for turbulent transfer in a stratified oceanic boundary layer. *J. Geophys. Res.*, **92,** 6977–6986.

——, 1990: Small scale processes. *Polar Oceanography,* W. Smith, Ed., Academic Press, 287–334.

——, 1991: Forced convection in the upper ocean near Fram Strait in late winter. *Deep Convection and Deep Water Formation in the Oceans,* P.-C. Chu and J.-C. Gascard, Eds., Elsevier, 69–86.

——, 1992: Turbulent heat flux in the upper ocean under sea ice. *J. Geophys. Res.*, **97,** 5365–5379.

——, and J. D. Smith, 1976: Measurements of the turbulent boundary layer under pack ice. *J. Phys. Oceanogr.*, **6,** 696–711.

——, and L. H. Kantha, 1989: Generation of internal waves by sea ice. *J. Geophys. Res.*, **94,** 3287–3302.

——, and D. G. Martinson, 1994: Turbulent mixing under drifting pack ice in the Weddell Sea. *Science,* **263,** 218–221.

——, G. A. Maykut, and J. H. Morison, 1987: Dynamics and thermodynamics of the ice/upper ocean system in the marginal ice zone of the Greenland Sea. *J. Geophys. Res.*, **92,** 7017–7031.

Mellor, G. L., and T. Yamada, 1982: Development of a turbulence closure model for geophysical fluid problems. *Rev. Geophys.*, **20,** 851–875.

Morison, J. H., M. G. McPhee, and G. A. Maykut, 1987: Boundary layer, upper ocean, and ice observations in the Greenland Sea marginal ice zone. *J. Geophys. Res.*, **92,** 6987–7011.

Moum, J. N., 1990: The quest for $K_\rho$—Preliminary results from direct measurements of turbulent fluxes in the ocean. *J. Phys. Oceanogr.*, **20,** 1980–1984.

Omstedt, A., and U. Svensson, 1984: Modeling supercooling and ice formation in a turbulent Ekman layer. *J. Geophys. Res.*, **89,** 735–744.

Padman, L., A. J. Plueddemann, R. D. Muench, and R. Pinkel, 1992: Diurnal tides near the Yermak Plateau. *J. Geophys. Res.*, **97,** 12 639–12 652.

Shay, T. J., and M. C. Gregg, 1986: Convectively driven turbulent mixing in the upper ocean. *J. Phys. Oceanogr.*, **16,** 1777–1798.

Shirasawa, K., 1986: Water stress and ocean current measurements under first-year sea ice in the Canadian Arctic. *J. Geophys. Res.*, **91,** 14 305–14 314.

Smith, N. R., and G. D. Hess, 1993: A comparison of vertical eddy mixing parameterizations for equatorial ocean models. *J. Phys. Oceanogr.*, **23,** 1823–1830.

Tennekes, H., 1973: The logarithmic wind profile. *J. Atmos. Sci.*, **30,** 234–239.

——, and J. L. Lumley, 1972: *A First Course in Turbulence.* The MIT Press, 300 pp.

Turner, J. S., 1973: *Buoyancy Effects in Fluids.* Cambridge University Press, 367 pp.

Wamser, C., and D. G. Martinson, 1993: Drag coefficients for winter Antarctic pack ice. *J. Geophys. Res.*, **98,** 12 431–12 437.

Zilitinkevich, S. S., 1975: Resistance laws and prediction equations for the depth of the planetary boundary layer. *J. Atmos. Sci.*, **32,** 741–752.

Zwally, H. J., and P. Gloersen, 1977: Passive microwave images of the polar regions and research application. *Polar Rec.*, **18,** 431–450.